Journal of Intelligent & Robotic Systems (2022) 104: 76
https://doi.org/10.1007/s10846-022-01583-7

SHORT PAPER

Hybrid Impedance-Sliding Mode Switching Control of the Indego Explorer Lower-Limb Exoskeleton in Able-Bodied Walking

Curt A. Laubscher[1] · Anthony Goo[1] · Ryan J. Farris[2] · Jerzy T. Sawicki[1]

Received: 3 August 2021 / Accepted: 21 January 2022 / Published online: 13 April 2022

Abstract

This paper proposes a novel hybrid controller for promoting safe human-robot interaction. The hybrid controller modifies a model-based impedance controller such that it uses impedance control but switches to sliding mode control under non-nominal conditions. Each control law is formulated with an inner-loop controller for feedback linearization and an outer-loop feedback controller for trajectory tracking. The outer-loop feedback torque is theoretically proven to have a smaller magnitude in hybrid control than in impedance control under an assumed condition, suggesting it may be the safer approach. To validate the mathematical assumption and purpose of the controller, a walking experiment is conducted where a healthy able-bodied subject using a lower-limb exoskeleton is randomly subjected to either hybrid or impedance control. Perturbations are induced through sudden changes in treadmill speed, resulting in operation outside nominal conditions for 15.9% of the experiment. The assumption made in the theory holds true for the majority of the experiment, failing only 14.3% of the time. The main results show a statistically significant reduction in average feedback torque magnitudes by 7.9%. This is accomplished without drastically affecting gait, with joint angle root-mean-square differences being 0.36° for the hip and 0.64° for the knee. This demonstrates how the hybrid controller can achieve similar gait patterns with lower feedback torque magnitudes, suggesting it is a promising alternative to impedance control.

Keywords Exoskeleton · Variable impedance control · Impedance control · Sliding mode control · Switching system · Safety

1 Introduction

Spinal cord injury (SCI) [1–3], traumatic brain injury (TBI) [4–6], stroke [7–9], and cerebral palsy (CP) [10] all represent afflictions and disorders which can result in lower-limb impairment, limited mobility, or paraplegia. Global epidemiological data show there are about 23 cases of SCI per million individuals with 180,000 new cases annually [3]. In North America, the incidence rates are larger at around 40 cases per million inhabitants [3]. A TBI can similarly result in motor neurological issues [4] and is an independent risk factor for stroke [5]. Epidemiological data for TBI indicate that there are around 81.1–97.9 incidences per million people per year [5]. In the United States alone, incidence rates are reportedly around 10.5 per million inhabitants per year [6] and prevalence data are estimated around 3.17 million individuals who live with permanent lasting effects from a TBI [5]. In developed countries, stroke is the leading contributor to long-lasting acquired disability, especially regarding functional mobility for walking and other activities of daily living [8, 9]. In the United States, there are about 0.5 million new cases of stroke every year [8] with around 26.9 survivors per million inhabitants [11]. CP is a group of brain lesion disorders during fetal or infant development that can result in a deficit in neuromotor control or in musculoskeletal impairment [10, 12, 13], which can negatively affect gait [12, 14]. In the

✉ Jerzy T. Sawicki
j.sawicki@csuohio.edu

Curt A. Laubscher
c.laubscher@csuohio.edu

Anthony Goo
a.goo@vikes.csuohio.edu

Ryan J. Farris
rfarris@messiah.edu

[1] Center for Rotating Machinery Dynamics and Control, Department of Mechanical Engineering, Cleveland State University, Cleveland, OH 44115-2214, USA

[2] Department of Engineering, Messiah University, Mechanicsburg, PA 17055-6706, USA

United States, CP is the most common cause for pediatric gait impairment, with about 3.1–3.6 cases for every 1000 children [15] and over 2.0 new cases for every 1000 live births [16]. SCI, TBI, stroke, CP, and other ailments can reduce functional mobility of a patient and thus their quality of life. However, recent studies have shown that increasing functional mobility through therapeutic and technological intervention can increase patient life satisfaction [2, 17].

Lower-limb exoskeletons are powered wearable robotic devices that provide supplemental torque at the joints of the user. Such devices can be used for robot-assisted gait training to rehabilitate ambulation for individuals with partial gait impairment [2, 8, 9], or for assistance to improve functional mobility in individuals with limited to no walking ability [1, 18]. Patients with SCI [1, 2, 18, 19], stroke [8, 9, 19–21], and TBI [20, 22] have used exoskeletons in clinical settings with varying degrees of success. Previous studies have shown that exoskeletons are generally safe to use [9, 19], with reported improvements in various measures of mobility and other outcomes. The 6-min walk test [9, 18] and timed up and go test [2, 9] are common methods for measuring outcomes, especially to quantify degree of mobility in individuals with paraplegia. Patient independence and mobility have been characterized using the functional independence measure [20, 22] and functional ambulation categories [2, 9], though others have been used as well [8]. Improvements in walking speed and endurance have also been reported [2, 8, 9]. Additionally, improvements in muscle strength [2], spasticity [2, 18], and bowel movement [18] are sometimes observed. Such articles highlight the benefits of exoskeletons in a clinical context. For more detailed descriptions and comparisons of exoskeleton hardware, see Refs. [23–27].

A common approach for control of exoskeletons is impedance-based control, which appears in the literature in various formulations [28–30]. Originally introduced in the series of seminal articles from Hogan [31–33], the controller is designed to enforce a specific dynamic relation between disturbances and the system response. This is employed in robotic systems to allow safe human-robot or environment-robot interactions through the allowance of some compliant behavior [30, 34]. The target impedance relation can be chosen as a second-order system with specified desired inertia, stiffness, and damping matrices. However, it is typical to make simplifications in the control law when applied in exoskeleton systems through the removal of disturbance feedback or inverse dynamics terms [30], drastically easing implementation details. Since some compliance is permitted, the controller does not strictly enforce a desired trajectory but rather applies a restoring control signal according to the desired impedance [28].

Variable-impedance controllers have been explored in the literature to adjust the target impedance relation during operation. Mohammadi and Gregg define their impedance parameters as periodic Bézier polynomials in terms of a state-dependent phase variable so that the parameters change across the gait cycle [35]. Yu et al. consider an impedance law formulated in Cartesian space with an adaptive neural network which varies the stiffness [36, 37]. Tran et al. varied impedance control parameters in stance and swing phase using fuzzy logic based on the system states and ground reaction force (GRF) data with their impedance relation defined using the human-exoskeleton joint angle differences rather than the system-reference joint angle errors [38]. Spyrakos-Papastavridis et al. developed a variable-impedance controller in Cartesian space specifically for preserving system passivity in compliant robotic systems [39].

This paper presents a hybrid impedance and sliding mode controller, extending our prior simulation work [40]. In brief, the proposed controller augments an impedance controller with a switching strategy that uses a sliding mode controller when the system is operating under non-nominal conditions. The controllers are formulated using identical inner-loop controllers for feedback linearization but different outer-loop controllers for trajectory tracking. The hybrid controller has been theoretically proven to conditionally have lower feedback control signal magnitudes than impedance control under non-nominal conditions, suggesting that the hybrid controller may be safer for human-robot interaction. The hybrid controller adds an extra layer of precaution to the model-based impedance controller by changing control approach when the states are far from the nominal operating region.

The contribution of this paper is to check if the theory of the hybrid controller holds true in experimental application to a human-exoskeleton system. Specifically, this paper examines the validity of an assumed mathematical inequality which is necessary for reducing feedback control signal magnitudes in the hybrid controller over the impedance controller, which was not explicitly validated in our prior work [40]. To make the results more interpretable, the theory is framed in this paper in terms of feedback torque rather than virtual acceleration which was considered in our prior work. In addition, this paper confirms the expected reduction in feedback torque magnitudes in experiment without greatly affecting gait tracking performance.

The content of this paper is as follows. First, the Indego Explorer, a lower-limb exoskeleton, is described and the dynamic model is derived using experimentally measured link parameters. To the authors' knowledge, this is the first publication explicitly characterizing the model of the Indego Explorer exoskeleton. Second, the theory of the hybrid controller is presented, which shows feedback torque magnitudes are conditionally lower than in impedance control under non-nominal conditions. The controller is then modified using a bilateral mixing strategy to allowing for a smooth, continuous transition during double limb support phase of gait. Third, the impedance controller and hybrid controller are both applied to

the exoskeleton in an able-bodied walking experiment under unperturbed and perturbed conditions with the results compared and discussed. This pilot work involves a single able-bodied subject for initial control application and theory validation prior to expanding to include more subjects. Fourth, limitations and future prospects are described. Finally, conclusions are discussed.

2 Indego Explorer Exoskeleton

2.1 Hardware Description and System Configuration

Similar to the Indego Therapy and Indego Personal exoskeletons [41, 42], the Indego Explorer exoskeleton is a powered lower-limb orthosis with actuated hip and knee joints with a pair of passive ankle-foot orthoses (AFOs) [43]. The Indego Personal device comes in only three separate sizes [44], whereas the Indego Therapy and Explorer exoskeletons both feature modular and adjustable link lengths, permitting individuals 1.55 to 1.91 m (5′ 1″ to 6′ 3″) in height and up to 113 kg (250 lb) in weight. The Explorer device distinguishes itself through its software and interface capabilities, and is intended to be used by researchers for investigational use. The Indego Explorer, depicted in Fig. 1, includes an optional functional-electrical stimulation capability, though this is not utilized in this work. The exoskeleton is reportedly capable of supplying torque upwards of 80 N·m at the hip and 51 N·m at the knee. Current command signals can be sent to the exoskeleton through a controller area network (CAN) bus. In this paper, the Simulink Desktop Real-Time toolbox in Matlab is configured to communicate with the exoskeleton for implementation of a current controller. Embedded electronics provide measurements of the joint angles, joint velocities, motor currents, and motor temperatures. In addition, inertial measurement units (IMU) located in the thigh components provide 3-axis accelerometer and gyroscopic data, which can be used for feedback in control.

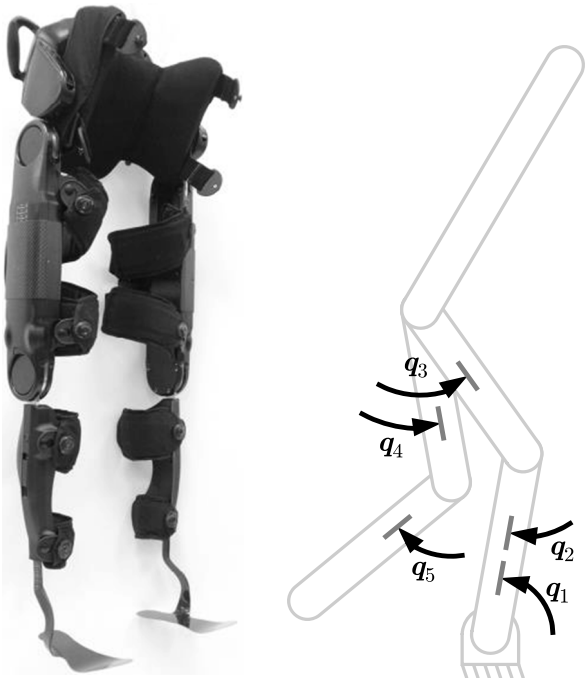

Fig. 1 The Indego Explorer exoskeleton has active hip and knee joints with passive ankle-foot orthoses to aid the subject in walking. The human-exoskeleton system can be modeled as a robotic system

For implementation, the hybrid and impedance controllers utilize vertical ground reaction force (GRF) data. The instrumented treadmill (Motek Medical) used in this paper provides analog values for the GRF, which are directly measured through a data acquisition and control system (dSPACE MicroLabBox DS1202). An interfacing computer running ControlDesk software is used for configuring and managing the dSPACE hardware. The dSPACE system is configured to communicate to the host computer using UDP/IP packets, sending the necessary GRF data for control feedback. A schematic outlining the hardware and how they communicate is depicted in Fig. 2.

2.2 Model Parameter Identification

Deriving a dynamic model of the Indego Explorer exoskeleton is necessary for implementation of model-based control strategies. The exoskeleton link lengths L were configured for compatibility with the subject and were recorded. The masses m of the exoskeleton components were measured using a scale. The centers of mass x of the parts in the distal-proximal direction were approximated by balancing the components.

The moments of inertia I of the components were measured using a trifilar pendulum [45, 46]. Each component with unknown inertia was placed on a rotating platform which was suspended in air by three supporting wires, as shown in Fig. 3. The rotational period T, inertia, and mass are related by

$$CT = \sqrt{\frac{I + I_0}{m + m_0}} = \rho \tag{1}$$

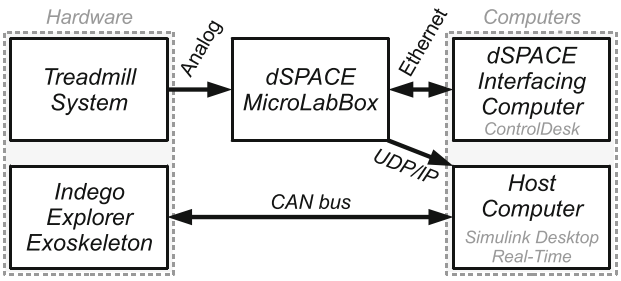

Fig. 2 Schematic of communicating systems

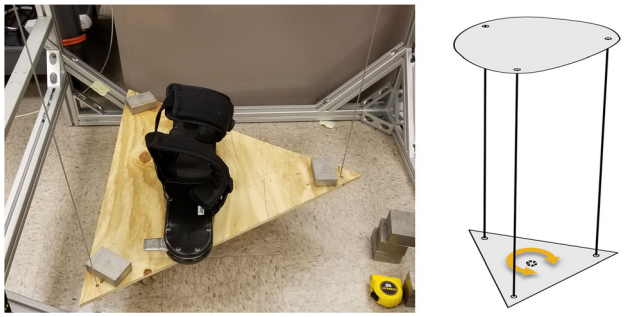

Fig. 3 Photograph of the trifilar pendulum experimental set-up and its schematic for moment of inertia identification

where C is a calibration coefficient, m_0 is the mass of the platform, I_0 is the inertia of the platform, and ρ is the radius of gyration for the entire platform-component system. The trifilar pendulum is calibrated using linear regression from measuring periods of the platform with steel blocks with known mass and inertia placed at known locations. The period of the system is taken with each component placed on the platform with the center of mass approximately located in the center. An average of 12 measurements was taken for each component and used to identify the radius of gyration for the net platform-component system and subsequently the inertia of each exoskeleton component. The calibration and identification data are shown in Fig. 4. The length, center of mass, mass, and moment of inertia for each exoskeleton component is listed in Table 1.

2.3 Human-Exoskeleton Dynamic Model

The dynamic model is composed of not only the exoskeleton components but also the body segments of the subject wearing the exoskeleton. Based on known basic subject information (male, 179 cm, 60 kg) and assuming body proportions and mass distribution from Winter [47], the human body segment parameters can calculated. Provided the exoskeleton is sufficiently tightened such that its components approximately move together with the body segments as rigid bodies, the parameters can be combined to form the parameters of the links in the human-exoskeleton model, which are summarized in Table 1.

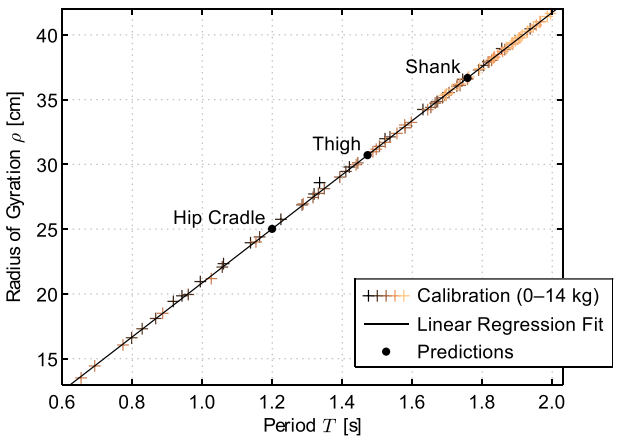

Fig. 4 Trifilar pendulum calibration and inertia identification for components of the exoskeleton

Table 1 Properties of the Indego Explorer exoskeleton components and the combined human-exoskeleton system links

Component/ Link	Length [m]	CoM[a] [m]	Mass [kg]	Inertia[b] [kg·m^2]
Hip Cradle	0.264[c]	0.155 H	7.06	0.102
Thigh	0.422	0.211 H	4.77	0.228
AFO (Shank)	0.444[d]	0.223 K	0.63	0.018
Trunk[e]	0.848[f]	0.293 H	48.57	2.081
Thigh	0.422	0.195 H	10.90	0.344
Shank[g]	0.444[d]	0.262 K	4.36	0.146

[a] Center of mass relative to hip (H) or knee (K) joint rotation axis

[b] Moment of inertia relative to center of mass

[c] Component length defined from hip joint rotation axis to top of hip cradle

[d] Component/link length defined from knee to ankle joint rotation axis

[e] Trunk link includes head, arms, torso, and hip cradle

[f] Trunk link length defined from hip joint rotation axis to top of head

[g] Shank link includes foot

With the link parameters known, the dynamic model can then be determined. For the purpose of this paper, a pinned-ankle model is used where one leg is on the ground with the ankle assumed to be pinned, and the other leg is free-floating. Using the Euler-Lagrange method, the tree-structure model is derived:

$$\mathbf{M}(\mathbf{q})\,\ddot{\mathbf{q}} + \mathbf{H}(\mathbf{q}) = \mathbf{u} + \mathbf{d} \tag{2}$$

where $\mathbf{q}$ is the configuration of the system defined in Fig. 1, $\mathbf{u}$ is the control input torques to the system, $\mathbf{d}$ is the disturbance torques acting on the system, $\mathbf{M}(\mathbf{q})$ is the configuration-dependent inertial matrix, and $\mathbf{H}(\mathbf{q})$ contains remaining terms in the dynamic model. For simplicity, joint friction is excluded from the model and the Coriolis-centrifugal term is neglected since speeds are assumed to be small. As such, $\mathbf{H}(\mathbf{q})$ only contains torques due to gravity and is independent of velocities.

3 Hybrid Impedance-Sliding Mode Control

The hybrid impedance-sliding mode control strategy in this paper is based on the controller proposed in our earlier work [40], which is reviewed here for completeness. The control strategy conditionally uses impedance control or sliding mode control. Both impedance control and sliding mode control can be formulated with a common inner-loop controller each with

a distinct outer-loop feedback controller, which is shown as a block diagram in Fig. 5.

The inner-loop controller is defined here as

$$\mathbf{u} = \mathbf{M}(\mathbf{q})\ddot{\mathbf{r}} + \mathbf{H}(\mathbf{q}) + \widetilde{\mathbf{u}} + \left(\mathbf{M}(\mathbf{q})\mathbf{M}_d^{-1} - \mathbf{I}\right)\mathbf{d} \tag{3}$$

where $\widetilde{\mathbf{u}}$ is the outer-loop feedback torque for trajectory tracking and $\mathbf{r}$ is the reference configuration to be tracked. Choosing $\widetilde{\mathbf{u}}=\mathbf{M}(\mathbf{q})\mathbf{v}$, the result of the inner-loop controller is feedback linearization where the system is transformed into a double-integrator system with virtual acceleration control input $\mathbf{v}$. An outer-loop feedback control law can be designed for controlling errors $\mathbf{e} = \mathbf{q} - \mathbf{r}$ for trajectory tracking. For this purpose, impedance and mode control are considered.

The feedback torque can be computed using the impedance control law.

$$\widetilde{\mathbf{u}}_{IC} = -\mathbf{M}(\mathbf{q})\mathbf{M}_d^{-1}(\mathbf{K}_d\mathbf{e} + \mathbf{D}_d\dot{\mathbf{e}}) \tag{4}$$

which, in combination with Eq. (3), is devised such that substitution in the plant model in Eq. (2) yields a closed-loop system satisfying the target impedance

$$\mathbf{d} = \mathbf{M}_d\ddot{\mathbf{e}} + \mathbf{D}_d\dot{\mathbf{e}} + \mathbf{K}_d\mathbf{e} \tag{5}$$

where $\mathbf{M}_d$, $\mathbf{D}_d$, and $\mathbf{K}_d$ are the positive definite matrices for desired inertia, damping, and stiffness, which are chosen control parameters.

The feedback torque can also be computed using the sliding mode control law

$$\widetilde{\mathbf{u}}_{SC} = -\mathbf{M}(\mathbf{q})\left(\mathbf{\Lambda}\dot{\mathbf{e}} + \gamma\frac{\mathbf{s}}{\|\mathbf{s}\|_{\mathbf{P}}}\right) \tag{6}$$

where $\|\mathbf{w}\|_{\mathbf{P}} = \sqrt{\mathbf{w}^{\mathrm{T}}\mathbf{P}\mathbf{w}}$ denotes the $\mathbf{P}$-norm of the arbitrary vector $\mathbf{w}$ for the chosen metric $\mathbf{P} = \mathbf{P}^{\mathrm{T}} \succ 0$, $\boldsymbol{s} = \mathbf{\Lambda}\mathbf{e} + \dot{\mathbf{e}}$ is the sliding variable, and $\gamma > 0$ and $\mathbf{\Lambda} = \mathbf{\Lambda}^{\mathrm{T}} \succ 0$ are both control parameters to be selected. In terms of the sliding variable, the closed-loop dynamics will satisfy

$$\mathbf{d} = \mathbf{M}_d\left(\dot{\mathbf{s}} + \gamma\frac{\mathbf{s}}{\|\mathbf{s}\|_{\mathbf{P}}}\right). \tag{7}$$

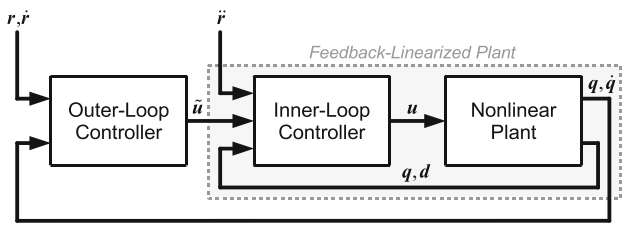

Fig. 5 Block diagram of the control architecture with an inner-loop feedback linearization controller and an outer-loop feedback controller to control the nonlinear plant

The impedance and sliding mode controllers only differ in the manner in which the feedback torque is computed. The hybrid impedance-sliding mode control strategy applied in this paper combines the two control strategies.

$$\widetilde{\mathbf{u}} = \begin{cases} \widetilde{\mathbf{u}}_{IC}, & \|\mathbf{s}\|_{\mathbf{P}} \le \alpha^{-1} \\ \widetilde{\mathbf{u}}_{SC}, & \|\mathbf{s}\|_{\mathbf{P}} > \alpha^{-1} \end{cases} \tag{8}$$

The premise of the hybrid controller is that the impedance controller will be used under normal operating scenarios where some disturbances are tolerated and minor deviation from the reference is permitted. However, if disturbances are larger than anticipated, then the system states can depart from the sliding manifold $\|\boldsymbol{s}\|_{\boldsymbol{P}} = 0$ by the switching threshold α. In this scenario, the hybrid controller will switch to a sliding mode controller, thereby limiting the magnitude of the control signals.

3.1 Parameter Constraints for Smooth Operation

The parameters in the impedance controller in Eq. (4), sliding mode controller in Eq. (6), and the hybrid control switching law in Eq. (8) should not be selected arbitrarily. Without special care, the control signal may chatter at the transition moment when $\|\mathbf{s}\|_{\mathbf{P}} = \alpha^{-1}$ due to repeated switching and a difference in torque values from the two controllers. To ensure the hybrid controller operates smoothly, the parameters should be chosen such that

$$\begin{aligned} \mathbf{M}_d^{-1}\mathbf{K}_d &= \alpha\gamma\mathbf{\Lambda} \\ \mathbf{M}_d^{-1}\mathbf{D}_d &= \alpha\gamma\mathbf{I} + \mathbf{\Lambda}. \end{aligned} \tag{9}$$

This is the control continuity condition and its satisfaction will guarantee the system will switch only once when entering the boundary layer without a change in the control signal when there are sufficiently small disturbances. This was derived and proven in Ref. [40] and is reiterated here in a concise manner for the simpler case without disturbances.

Consider states in the neighborhood of the boundary layer $\|\mathbf{s}\|_{\mathbf{P}} = \alpha^{-1}$. The difference between the control signal on either side will be

$$\begin{aligned} \Delta\mathbf{u} &= \mathbf{u}_{IC} - \mathbf{u}_{SC} \\ &= -\mathbf{M}(\mathbf{q})\mathbf{M}_d^{-1}(\mathbf{K}_d\mathbf{e} + \mathbf{D}_d\dot{\mathbf{e}}) + \mathbf{M}(\mathbf{q})\mathbf{\Lambda}\dot{\mathbf{e}} + \gamma\mathbf{M}(\mathbf{q})\mathbf{s}/\|\mathbf{s}\|_{\mathbf{P}} \\ &= \mathbf{M}(\mathbf{q})\left(\left(\alpha\gamma\mathbf{\Lambda} - \mathbf{M}_d^{-1}\mathbf{K}_d\right)\mathbf{e} + \left(\alpha\gamma\mathbf{I} + \mathbf{\Lambda} - \mathbf{M}_d^{-1}\mathbf{D}_d\right)\dot{\mathbf{e}}\right) \end{aligned}$$

which will equal zero when Eq. (9) is satisfied. As such, the control signal does not change and therefore will be continuous when crossing the boundary layer.

Next is to show the system will switch only once when at the boundary layer. First, consider the case when sliding mode

control is active. Define the Lyapunov-like function

$$V = \frac{1}{2}\|\mathbf{s}\|_{\mathbf{P}}^2$$

Taking the time derivative and substituting in the closed-loop dynamics from Eq. (7) gives

$$\dot{V} = \mathbf{s}^{\mathrm{T}}\mathbf{P}\dot{\mathbf{s}} = -\gamma\|\mathbf{s}\|_{\mathbf{P}}$$

which will be negative. This shows $\|\mathbf{s}\|_{\mathbf{P}}$ will be decreasing when sliding mode control is active with states on the boundary layer. The system will always switch from sliding mode control to impedance control.

When states are inside the boundary layer and impedance control mode is active, the hybrid controller will use impedance control even in the presence of some disturbances. An additional constraint is applied to ensure the states remain within the threshold $\|\mathbf{s}\|_{\mathbf{P}} < \alpha^{-1}$ in the presence of bounded disturbances.

$$\begin{bmatrix} -\boldsymbol{\Lambda}\mathbf{R} - \mathbf{R}\boldsymbol{\Lambda} + \mu\mathbf{R} & \alpha^{-2}\mathbf{P}^{-1} \\ \alpha^{-2}\mathbf{P}^{-1} & (\mu - 2\alpha\gamma)\alpha^{-2}\mathbf{P}^{-1} + \frac{1}{\mu}\mathbf{M}_d^{-1}\mathbf{D}\mathbf{M}_d^{-1} \end{bmatrix} \prec 0 \tag{10}$$

Satisfaction of this matrix inequality for some $\mathbf{R} = \mathbf{R}^{\mathrm{T}} \succ 0$ and $\mu > 0$ will guarantee the set of states satisfying $\|\mathbf{s}\|_{\mathbf{P}} < \alpha^{-1}$ is a robust invariant set for disturbances satisfying $\mathbf{d}^{\mathrm{T}}\mathbf{D}^{-1}\mathbf{d} \leq 1$ [40]. By assigning μ iteratively in a search space and by choosing $\mathbf{R}$ and $\mathbf{D}$ as decision variables, this can be solved with a linear matrix inequality (LMI) solver. Minimization of the objective function $J = \varepsilon\ \mathrm{tr}(\mathbf{R}) - \mathrm{tr}(\mathbf{D})$ for a small $\varepsilon > 0$ will have the effect of determining the maximum permitted disturbances for a given controller where $\mathrm{tr}(\cdot)$ denotes the trace function. This process can be used to determine the disturbance magnitude a given controller will permit.

Interestingly, the closed-loop dynamics of the sliding mode controller can be written in a form similar to Eq. (5) with identical inertia matrix but with differing damping and stiffness matrices. Provided the control continuity condition in Eq. (9) is satisfied, the closed-loop dynamics would be

$$\mathbf{d} = \mathbf{M}_d\ddot{\mathbf{e}} + (\kappa\mathbf{D}_d + (1-\kappa)\boldsymbol{\Lambda})\dot{\mathbf{e}} + (\kappa\mathbf{K}_d)\mathbf{e}. \tag{11}$$

where $\kappa = 1/(\alpha\|\mathbf{s}\|_{\mathbf{P}})$. When inside the boundary layer ($\kappa > 1$), the closed-loop dynamics would have the desired inertia, stiffness, and mass matrices as in Eq. (5). However, when the states are outside the boundary layer ($0 < \kappa < 1$) and are progressively getting further from the manifold, the stiffness matrix would decrease proportionally from $\mathbf{K}_d$, and the damping matrix would approach $\boldsymbol{\Lambda}$. As such, the hybrid controller can be considered as a variable-impedance controller.

3.2 Safety Consideration

With a pure impedance control approach, large errors in reference tracking performance can result in large feedback torque control signal magnitudes. For instance, this can arise in scenarios when joint motion is desynchronized from the reference trajectory, large disturbances are encountered, or control is implemented incorrectly. This may result in unexpected system behavior, possibly damaging the hardware or injuring the patient using the exoskeleton. Safe control design is a crucial consideration for the practical use of exoskeletons. The hybrid impedance-sliding mode switching control strategy adds a layer of precaution to a traditional model-based impedance controller by changing strategies when the system states are far from the nominal operational region.

Intuition suggests that the normalization of the sliding variable in the sliding mode controller in Eq. (6) will limit the magnitude of the control signals, at least for that one term. Indeed, it has been shown that the virtual acceleration control signal magnitudes in sliding mode control are conditionally lower than that of impedance control when the states are outside the boundary layer [40]. This paper finds a similar condition but for comparing feedback torques by assuming

$$A(\mathbf{q},\mathbf{s},\dot{\mathbf{e}}) = 2\mathbf{s}^{\mathrm{T}}\widetilde{\mathbf{P}}(\mathbf{q})\boldsymbol{\Lambda}\dot{\mathbf{e}} + \gamma\left(\alpha + 1/\|\mathbf{s}\|_{\mathbf{P}}\right)\mathbf{s}^{\mathrm{T}}\widetilde{\mathbf{P}}(\mathbf{q})\mathbf{s} > 0 \tag{12}$$

holds true where $\widetilde{\mathbf{P}}(\mathbf{q}) = \mathbf{M}(\mathbf{q})\mathbf{P}\mathbf{M}(\mathbf{q})$. Provided this inequality is satisfied, then sliding mode control will give smaller feedback torque magnitudes than impedance control when outside the manifold, which will be proven below. Applying the assumption that states are outside the boundary layer so that $\|\mathbf{s}\|_{\mathbf{P}} > \alpha^{-1}$, then Eq. (12) implies

$$\begin{aligned}
&2(\alpha - 1/\|\mathbf{s}\|_{\mathbf{P}})\mathbf{s}^{\mathrm{T}}\widetilde{\mathbf{P}}\boldsymbol{\Lambda}\dot{\mathbf{e}} > -\gamma(\alpha + 1/\|\mathbf{s}\|_{\mathbf{P}})(\alpha - 1/\|\mathbf{s}\|_{\mathbf{P}})\mathbf{s}^{\mathrm{T}}\widetilde{\mathbf{P}}\mathbf{s} \\
&2\gamma(\alpha - 1/\|\mathbf{s}\|_{\mathbf{P}})\mathbf{s}^{\mathrm{T}}\widetilde{\mathbf{P}}\boldsymbol{\Lambda}\dot{\mathbf{e}} > \gamma^2\left(1/\|\mathbf{s}\|_{\mathbf{P}}^2 - \alpha^2\right)\mathbf{s}^{\mathrm{T}}\widetilde{\mathbf{P}}\mathbf{s} \\
&2\alpha\gamma\mathbf{s}^{\mathrm{T}}\widetilde{\mathbf{P}}\boldsymbol{\Lambda}\dot{\mathbf{e}} - 2\gamma(1/\|\mathbf{s}\|_{\mathbf{P}})\mathbf{s}^{\mathrm{T}}\widetilde{\mathbf{P}}\boldsymbol{\Lambda}\dot{\mathbf{e}} > (\gamma/\|\mathbf{s}\|_{\mathbf{P}})^2\mathbf{s}^{\mathrm{T}}\widetilde{\mathbf{P}}\mathbf{s} - (\alpha\gamma)^2\mathbf{s}^{\mathrm{T}}\widetilde{\mathbf{P}}\mathbf{s} \\
&(\alpha\gamma)^2\mathbf{s}^{\mathrm{T}}\widetilde{\mathbf{P}}\mathbf{s} + 2\alpha\gamma\,\mathbf{s}^{\mathrm{T}}\widetilde{\mathbf{P}}\boldsymbol{\Lambda}\dot{\mathbf{e}} + > \dot{\mathbf{e}}^{\mathrm{T}}\boldsymbol{\Lambda}\widetilde{\mathbf{P}}\boldsymbol{\Lambda}\dot{\mathbf{e}} > \ldots \\
&(\gamma/\|\mathbf{s}\|_{\mathbf{P}})^2\mathbf{s}^{\mathrm{T}}\widetilde{\mathbf{P}}\mathbf{s} + 2\gamma(1/\|\mathbf{s}\|_{\mathbf{P}})\mathbf{s}^{\mathrm{T}}\widetilde{\mathbf{P}}\boldsymbol{\Lambda}\dot{\mathbf{e}} + \dot{\mathbf{e}}^{\mathrm{T}}\boldsymbol{\Lambda}\widetilde{\mathbf{P}}\boldsymbol{\Lambda}\dot{\mathbf{e}} \\
&(\alpha\gamma\mathbf{s} + \boldsymbol{\Lambda}\dot{\mathbf{e}})^{\mathrm{T}}\widetilde{\mathbf{P}}(\alpha\gamma\mathbf{s} + \boldsymbol{\Lambda}\dot{\mathbf{e}}) > (\gamma\mathbf{s}/\|\mathbf{s}\|_{\mathbf{P}} + \boldsymbol{\Lambda}\dot{\mathbf{e}})^{\mathrm{T}}\widetilde{\mathbf{P}}(\gamma\mathbf{s}/\|\mathbf{s}\|_{\mathbf{P}} + \boldsymbol{\Lambda}\dot{\mathbf{e}})
\end{aligned}$$

Assuming the continuity condition in Eq. (9) is satisfied, then

$$\begin{gathered}
\left\|\mathbf{M}(\mathbf{q})\left(\mathbf{M}_d^{-1}\mathbf{K}_d\mathbf{e} + \mathbf{M}_d^{-1}\mathbf{D}_d\dot{\mathbf{e}}\right)\right\|_{\mathbf{P}}^2 > \left\|\mathbf{M}(\mathbf{q})\left(\gamma\mathbf{s}/\|\mathbf{s}\|_{\mathbf{P}} + \boldsymbol{\Lambda}\dot{\mathbf{e}}\right)\right\|_{\mathbf{P}}^2 \\
\left\|\widetilde{\mathbf{u}}_{IC}\right\|_{\mathbf{P}} > \left\|\widetilde{\mathbf{u}}_{SC}\right\|_{\mathbf{P}}
\end{gathered} \tag{13}$$

This concludes the proof that the feedback torques from the impedance control signal exceeds that of the sliding mode control signal under certain conditions. If the states are outside

the boundary layer, if the continuity condition in Eq. (9) is satisfied, and if the assumption in Eq. (12) is satisfied, then sliding mode control will yield lower feedback torque magnitudes than impedance control for the given states. A similar analysis can show that the inverse holds, where states inside the boundary layer implies sliding mode control would yield greater feedback torque magnitudes than impedance control. However, sliding mode control will be inactive whenever the states are within the manifold.

3.3 Bilateral Mixing Control

The controller described earlier in Section 3 assumes the dynamics of the system can be modeled in the form of Eq. (2). This will hold true for a large proportion of the full gait cycle, namely during single limb support when only one foot is in contact with the ground and supporting the body. However, for nearly a quarter of the entire gait cycle, both feet are in contact with the ground [48] and the pinned foot assumption will not be wholly accurate.

Ideally, the transition between the two single limb support phases will be seamless for the operator. The authors elected against using a finite-state machine as the discrete events would result in a discontinuous change in control signal. Rather than an instantaneous switch, two identical hybrid controllers are combined using a bilateral mixing strategy [49]. The bilateral mixing controller is defined as

$$\mathbf{u} = w_{\mathrm{L}}\mathbf{u}_L + w_{\mathrm{R}}\mathbf{u}_R \tag{14}$$

where $\mathbf{u}_L$ and $\mathbf{u}_R$ are the control torque signals under the assumption that the left or right foot is on the ground as calculated from Eq. (3). The weighted sum of these signals is taken in Eq. (14) where w_{L} and w_{R} are the coefficient weights calculated from normalized vertical GRF.

$$w_{\mathrm{L/R}} = \begin{cases} \dfrac{f_{\mathrm{L/R}}}{f_{\mathrm{L}} + f_{\mathrm{R}}}, & f_{\mathrm{L}} + f_{\mathrm{R}} \not\approx 0 \\ 0, & f_{\mathrm{L}} + f_{\mathrm{R}} \approx 0 \end{cases} \tag{15}$$

When at least one foot is on the ground, the weights w_{L} and w_{R} are respectively proportional to the measured vertical GRF f_{L} and f_{R} such that $w_{\mathrm{L}} + w_{\mathrm{R}} = 1$ and $0 \leq w_{\mathrm{L/R}} \leq 1$. In the uncommon case when neither foot is on the ground, the weights are $w_{\mathrm{L}} = w_{\mathrm{R}} = 0$ so no control input is applied. The block diagram depicting the combination of the two controllers is shown in Fig. 6.

When only one foot is in contact with the ground, all weight is put into the controller that assumes the respective foot is pinned. When both feet are in contact with the ground, the weight distributed among the two legs according to the measured GRF. This approach allows for a smooth, continuous control signals throughout the entire gait motion, even during double limb support. As one foot comes into contact with the ground and later is removed from the ground, the corresponding weight coefficient will increase from zero, reach and hold at one, and then decrease until it reaches zero again. Since the exoskeleton is uncontrolled at the ankle, the stance ankle control signal is ignored in application.

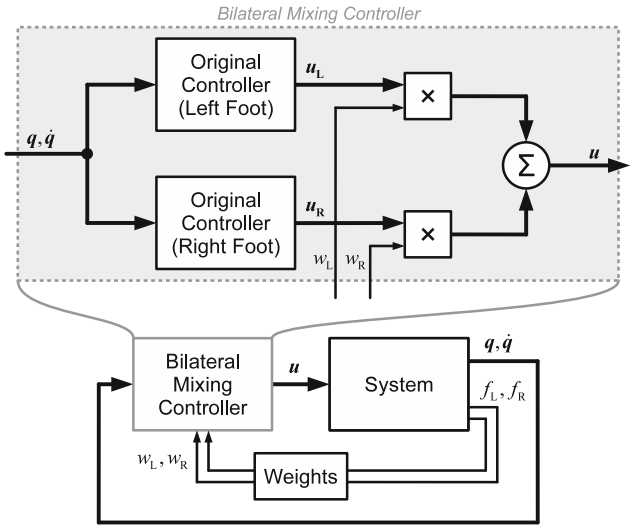

Fig. 6 Block diagram of the bilateral mixing controller consists of a weighted sum of the two original control laws, each assuming one or the other foot is pinned

4 Experimental Validation

4.1 Procedure and Methods

A single able-bodied subject (male, 29 years, 60 kg, 180 cm) is used for experimental evaluation of the hybrid controller in level treadmill walking, shown in Fig. 7. Since the proposed

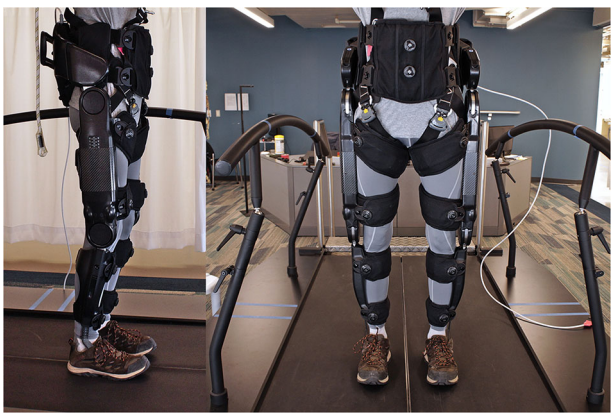

Fig. 7 Experimental setup. The experiment entails walking on a treadmill while being assisted by the Indego Explorer exoskeleton by the hybrid or impedance controller

hybrid controller is developed such that it differs from impedance control only when outside nominal operation, a perturbation signal is applied to disturb the system while the subject walks on the treadmill to impose non-nominal conditions. The experimental procedure consists of the subject walking on the treadmill, alternating between perturbed and unperturbed conditions every minute for a duration of 12 min. Impedance control and hybrid control are chosen randomly every third gait cycle, and the subject is blind to which controller is used. The subject is strapped into a safety harness as precautionary measure. The reference trajectory utilized by the controller is a predesignated gait pattern with constant period. To synchronize the subject motion with the exoskeleton reference trajectory, a metronome is used to indicate heel-strike timing.

The perturbations are chosen as a sequence of timed step changes in treadmill speed, thereby applying an anterior-posterior disturbance. Here, the sequence is chosen as a maximum length pseudo-random binary sequence (PRBS) [50, 51]. This is chosen due to having the desirable properties of being reproducible and exciting the system up to a designed frequency. A PRBS-k signal is periodic with $n = 2^k - 1$ elements spaced by a chosen time step Δ. The Fourier transform of this signal follows the absolute value of the sinc function at integer multiples of $1/(n\Delta)$, and is equal to zero elsewhere. For this paper, a PRBS-6 signal is selected, listed as A011673 on the On-Line Encyclopedia of Integer Sequences [52]. A time step of $\Delta = 0.1$ s is chosen so that the signal excites frequencies up to around 4.42 Hz at the −3 dB cutoff frequency. The theoretical frequency response is depicted in Fig. 8.

The base treadmill speed is selected as 0.28 m/s, chosen based on subject preference when walking with the controlled exoskeleton. The perturbation magnitude is selected as 0.20 m/s peak-to-peak with a mean value equal to the base treadmill speed. The perturbation magnitude creates minor stumbles and increases the proportion of time under non-nominal operation where $\|\mathbf{s}\|_{\mathbf{P}} > \alpha^{-1}$ without risking loss of balance or falls.

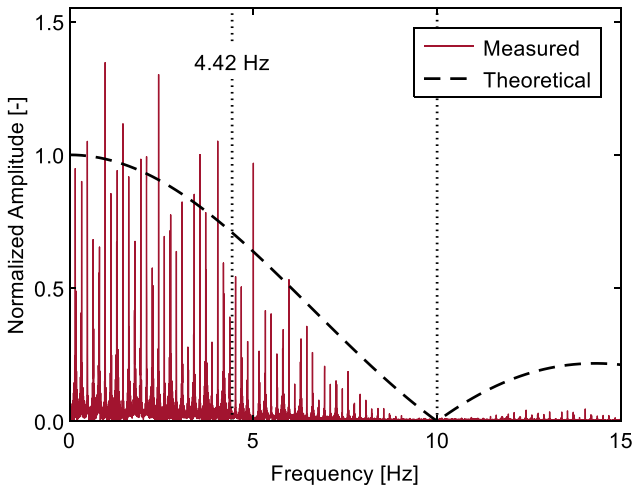

Fig. 8 The Fourier transform of the PRBS-6 signal follows the absolute value of a scaled sinc function at discrete points. The measured value deviates from the theoretical and rolls off due to measurement aliasing and noise, and imperfect tracking of the desired treadmill speed profile

To use the hybrid and impedance controllers, a reference trajectory is required. An unperturbed walking experiment is conducted with 60% partial gravity compensation for the full system. This control strategy was chosen since it does not require a reference trajectory while still mitigating the affects from wearing the exoskeleton to some degree. The gait data recorded by the exoskeleton are partitioned into full gait cycles using GRF measurements and underwent ensemble averaging. A piecewise polynomial with periodic constraints is subsequently fit to each of the three signals, namely shank orientation, knee angle, and hip angle. These functions are used as the reference trajectory in the main experiment.

The perturbation magnitude and control parameters are selected together and iteratively. The hybrid control parameters are chosen initially based on user comfort. The parameters $\mathbf{P}$ and $\mathbf{\Lambda}$ are tuned such that the position and velocity errors roughly contribute equally to $\|\mathbf{s}\|_{\mathbf{P}}$ under the perturbation condition throughout locomotion. Since $\mathbf{P}$ is used as a tuning parameter in this paper, that made the switching threshold α redundant so it was chosen as 1 without loss of generality. The value of γ is then chosen based on user comfort. The value of $\mathbf{M}_d$ is chosen to be the diagonal elements of $\mathbf{M}(\mathbf{q}_0)$ using the model of the human-exoskeleton system where $\mathbf{q}_0$ is the upright standing configuration. This made the disturbance feedback term in the control law negligible, so they were excluded in implementation. The remaining control parameters $\mathbf{K}_d$ and $\mathbf{D}_d$ are computed such that the continuity condition in Eq. (9) is satisfied. The parameters in the impedance controller are chosen as the identical impedance parameters used by the hybrid controller. A summary of the control parameters can be found in Table 2. The parameters for the five degrees of freedom correspond to the configuration variables in the model in Eq. (2) and are depicted in Fig. 1. The transition of the control signal between stance and swing phase is made continuous through Eq. (14).

Given the control parameters, the permitted disturbances are calculated using Eq. (10) and are included in Table 2. Complete feedback linearization proved impractical in experimental application, so coefficients are introduced to scale down the control signal: 30% for the feedforward term and 60% for the gravity compensation term. To avoid the feedforward term applying large torques resulting from imperfect heel-strike and toe-off timing with the incorrect pinned-ankle assumption, its torque is also scaled by a reference weight, found in a similar manner to the derivation of the reference trajectory. As an extra layer of precaution, exoskeleton torques are saturated at 35 N·m.

Table 2 Summary of control parameters and permitted disturbances

Parameter [Units]		Stance Shank	Stance Knee	Stance Hip	Swing Hip	Swing Knee
$\mathbf{P}$	[s^2/rad^2]	0.7	0.3	1.6	1.8	0.34
$\mathbf{\Lambda}$	[1/s]	1.25	1.25	3.75	2.50	2.50
$\mathbf{M}_d$	[kg·m^2]	77.80	28.75	8.90	2.64	0.29
$\mathbf{K}_d$	[N·m/rad]	58.35	21.56	20.03	3.96	0.43
$\mathbf{D}_d$	[N·m·s/rad]	143.93	53.18	38.72	8.18	0.90
$\sqrt{\mathbf{D}}$	[N·m]	39.1	9.4	6.8	2.1	0.1

All matrices are diagonal with elements tabulated. The scalar control parameters are $\alpha = 1.0$ and $\gamma = 0.6\ s^{-1}$

4.2 Results and Discussion

Following the procedure described in Section 4.1, an experiment was conducted to evaluate the hybrid controller and compare it to an impedance controller. The 12-min portion of the experiment used in data acquisition and analysis is shown in Fig. 9. A fast-Fourier transform of the treadmill speed was performed and has been included in Fig. 8. As shown in the detailed view in Fig. 9, the treadmill followed the PRBS reference speed adequately well to perturb the subject when walking, with occasional minor stumbles. The subject commented that it was more difficult to walk and had to especially concentrate on walking during the perturbed condition than during the unperturbed condition.

The gait motion for the perturbed condition is shown in Fig. 10 for a full gait cycle with the reference gait obtained from the pure gravity compensation experiment included. The joint angles roughly resemble those of standard gait recorded from a healthy population as reported by Winter [53] with a couple notable exceptions. The knee does not exhibit the typical flexion peak during stance phase, and hip motion is less pronounced during stance phase than in natural gait. A disparity between the reference gait and natural walking motion is not surprising as the subject was burdened by wearing an exoskeleton in the experiment conducted for obtaining the reference gait. There was an imperfect, non-rigid fixation between the subject and the exoskeleton, particularly at the hip cradle. Additionally, stance knee motion was likely reduced since the torque from the subject at push-off was diminished by the passive AFO in the exoskeleton. All these factors combine to cause discrepancies between the recorded reference gait and an unburdened nominal gait pattern.

In the control experiment, the hybrid controller and impedance controller had very similar gait patterns. The RMS difference in average joint angles is merely 0.36° for the hip and 0.64° for the knee. This is promising as it suggests the hybrid controller performs similarly in gait tracking to the impedance controller. For the perturbation condition, the disturbances did not result in a consistent change in the ensemble average in joint angles. This is

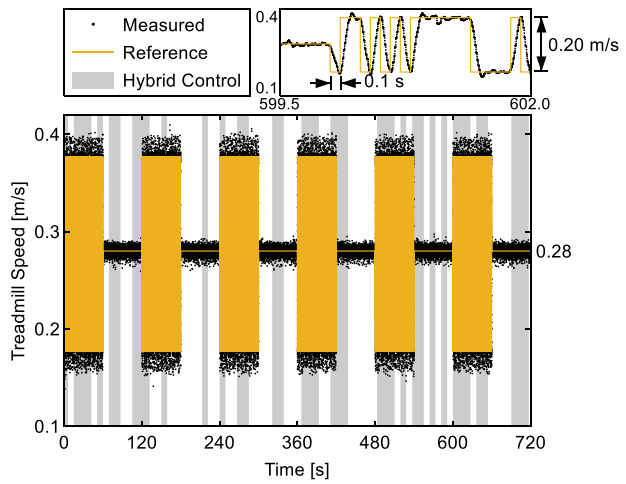

Fig. 9 The treadmill speed throughout the experimental procedure. The speed alternates between perturbed and unperturbed with a randomly selected control mode every 3 gait cycles, either hybrid control (highlighted) or impedance control (not highlighted)

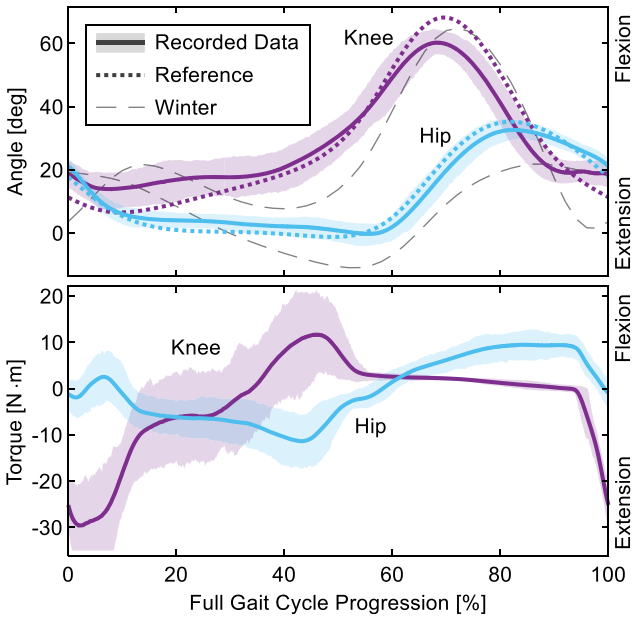

Fig. 10 Experimental results for the perturbed condition. The ensemble average of gait and control torque are shown, with upper and lower decile bounds. The reference trajectory used in control and Winter data are included

revealed in the root-mean-square (RMS) difference between the perturbed and unperturbed joint angle ensemble average being only 0.67° for the hip and 1.3° for the knee. This is unsurprising since the perturbations were random and effects tended to average out to marginal changes in the ensemble average across many gait cycles. Although the average gait pattern was not drastically affected, the variability in gait did increase. Table 3 quantifies the variability in joint angles and torques as the square root of the mean variance (RMV) and the coefficient of variation (CV) [53]. Similar to the joint angles, the variability in the torque levels increased from the unperturbed condition to the perturbed condition. The increase in gait variability is expected since perturbations tend to result in motion differing from the desired motion more so than the baseline variability observed in the unperturbed data. The increase in control torque variability is due to its dependence on the gait.

Although the controller was randomly assigned to either hybrid or impedance control throughout the experiment, the subject did not notice any of these changes. This is unsurprising since the two control strategies give identical torque values under nominal conditions when $\|\mathbf{s}\|_{\mathbf{P}} < \alpha^{-1}$ and give similar torque values when $\|\mathbf{s}\|_{\mathbf{P}} \gtrsim \alpha^{-1}$ due to being continuous when crossing the boundary layer. The two strategies only differ to a large degree when far outside the boundary layer $\|\mathbf{s}\|_{\mathbf{P}} \gg \alpha^{-1}$, which did not occur very frequently. This is evidenced by Fig. 11, showing the norm of the sliding variable throughout gait and the proportion of gait cycles in which it is outside the boundary layer. Only stance phase is depicted since the ipsilateral controller is inactive during swing phase with only the contralateral controller contributing torques due to Eq. (14). Both controllers contribute during double limb support. The beginning portion spans from ipsilateral heel-strike defined at 0% until contralateral toe-off at 17.9 ± 2.2% (mean ± standard deviation), and the ending portion spans from contralateral heel-strike at 82.5 ± 2.0% until ipsilateral toe-off defined at 100%. The ensemble average of $\|\mathbf{s}\|_{\mathbf{P}}$ is above α^{-1} for 15.9% of the stance phase, though the upper and lower decile bounds and the proportion graph show the states escape the boundary layer at other moments throughout gait as well. The exact moment will depend on factors like natural subject variability in gait and, more importantly, perturbation timing. The gait may be more sensitive to the

Table 3 Variation of joint angles and torque

Joint	Condition	Angle RMV (CV)	Torque RMV (CV)
Hip	Unperturbed	2.05° (0.166)	2.5 N·m (0.391)
Hip	Perturbed	2.73° (0.226)	3.1 N·m (0.517)
Knee	Unperturbed	3.45° (0.118)	3.7 N·m (0.521)
Knee	Perturbed	4.89° (0.170)	5.3 N·m (0.751)

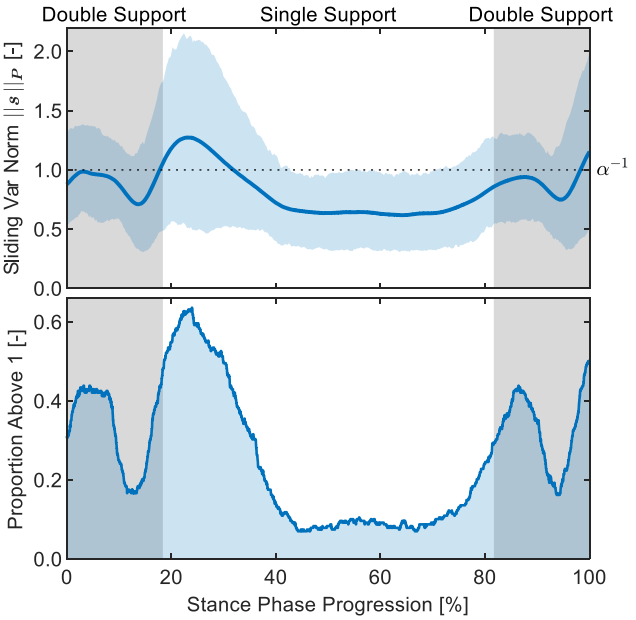

Fig. 11 Ensemble average of the sliding variable norm and the proportion of gait cycles in which the error states were outside the boundary layer under the perturbed condition. Bounds are defined by upper and lower deciles

perturbations depending on the configuration of the system. A sudden change in treadmill speed soon before heel-strike could change foot step timing. This likely explains the peaks in proportion soon after ipsilateral heel-strike at 5.0%, contralateral toe-off at 23.9% and contralateral heel-strike at 86.5%, as well as around ipsilateral toe-off at 100.0%.

One objective of this paper is to experimentally check if the assumed condition $A(\mathbf{q}, \mathbf{s}, \dot{\mathbf{e}}) > 0$ in Eq. (12) holds true in the context of gait control in a human-exoskeleton system. Figure 12 depicts the value of this function throughout locomotion and the proportion of gait cycles in which it is negative. The assumption seems to fail infrequently as the ensemble average remains positive for the entirety of the stance phase, though the decile bounds indicate the assumption does fail for some gait cycles, especially at particular moments. Failure occurs most frequently soon after contralateral toe-off at 20.5% of stance phase and soon before ipsilateral toe-off at 98.6%. In either case, this could conceivably have an effect on the feedback torque inequality in Eq. (13), but the latter case is immaterial since the bilateral mixing controller weight coefficient in Eq. (14) is nearing zero here. Furthermore, the assumption failed only 14.3% of the entirety of the perturbed condition. Taken altogether, the assumption in Eq. (12) tends to hold true most of the time, with failure occurring most frequently around toe-off of either leg.

The feedback torque magnitudes of the hybrid and impedance controllers are compared in Fig. 13. The ensemble average of $\|w\tilde{\mathbf{u}}\|_{\mathbf{P}}$ is greater in impedance control than in hybrid control for 80.6% of the gait, showing how the feedback torques tend to be lower in the hybrid controller. This

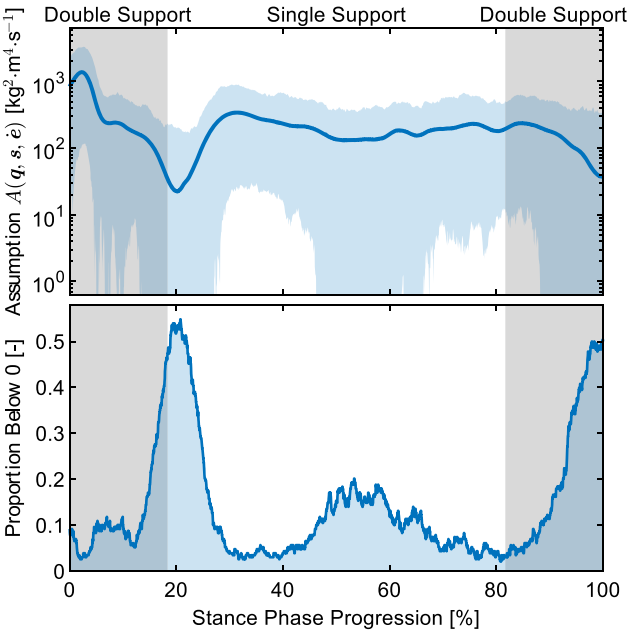

Fig. 12 Ensemble average of the positive assumption function from Eq. (12) and the proportion of gait cycles in which it is dissatisfied (negative) in the perturbation condition. Bounds are defined by upper and lower deciles

confirms the theory that the feedback torque magnitudes of the hybrid controller are lower than that of the impedance controller. The reason this did not hold for the entirety of stance phase is twofold. First, an assumption was made in Eq. (12), though it has been shown earlier to remain valid

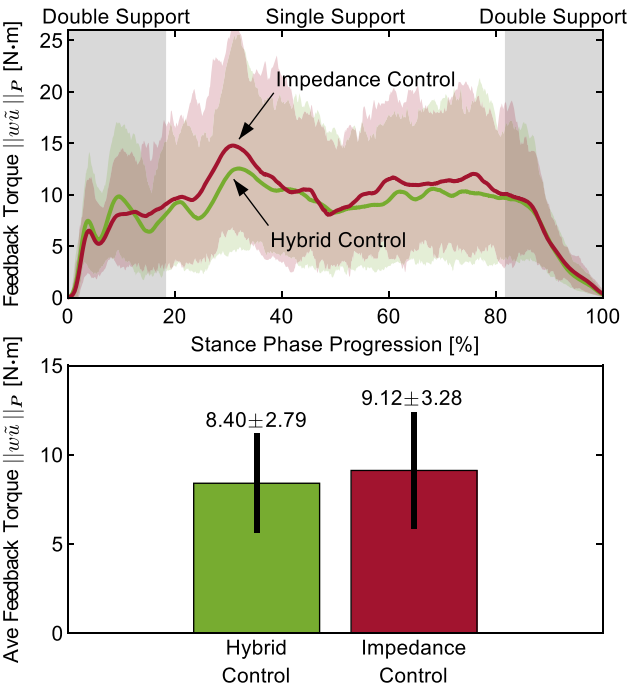

Fig. 13 Comparison of feedback torque control signals for the perturbed condition. Time-dependent values include upper and lower decile bounds, and time-average values show mean and standard deviations

the majority of the time. Second, the theoretical proof comparing feedback torques assumed the same system states so the gaits would have to be identical, though the similarity between the two gaits was quantified earlier and was shown to be small. To quantify the degree in which feedback torques differ between the two control strategies, the average value is taken throughout the gait cycles and are also shown in Fig. 13. Performing a t-test with significance level of 0.05, a statistically significant change in feedback torque was observed ($p = 0.0015$). The 7.9% lower feedback torque magnitudes in hybrid control than impedance control suggest that the hybrid controller successfully reduces torque levels when performing gait tracking.

5 Limitations and Future Work

There are a few limitations of the presented research which provide possible directions for future work. First, the incomplete feedback linearization changes the interpretation of the disturbances in Table 2 calculated from the LMI in Eq. (10). In application, complete feedback linearization proved difficult as the subject would be fighting the exoskeleton. For practical implementation, coefficients were introduced to scaled down the control signals. However, the theory that led to the derivation of the LMI assumes complete feedback linearization with disturbance feedback, where gravity is fully compensated and the feedforward term is not scaled down. Future work entails investigating how inaccuracies in these assumptions can be lumped into the value of the disturbances. Second, although the theory guarantees feedback torque magnitudes will be lower in hybrid control than in impedance control, this assumes identical gait patterns. Subject gait patterns could change between the two control strategies such that larger feedback torque magnitudes are possible in hybrid control, though this was not generally observed in the presented results. Third, the subject relied on the handrails for lateral balance, introducing subject-environment interactions which can be considered disturbances on the system. Use of the handrails was necessary for practical application of the exoskeleton since the device restricts the hip adduction-abduction motions. Future work includes applying the presented controller with alternate exoskeleton hardware currently under development without this limitation [54, 55]. Fourth, a limitation of the theory is the continuity condition in Eq. (9), which gave much larger derivative gains than proportional gains and could result in undesirable oscillatory motion if the gains were too high. Variations on the proposed controller can be investigated that do not have this limitation. Fifth, a limitation of the proposed controller for exoskeleton systems is the necessity of GRF feedback. The

exoskeleton in this paper did not have integrated GRF sensors and relied on measurements via other means, namely the instrumented treadmill, which limits the applicability to within the testing facility. Future work entails integration of GRF sensors with the exoskeleton to permit use of the control strategy in other environments.

It is important not to overgeneralize the results as the conducted experiments in this paper are only for a single subject and consider a single measure of safety. It remains to be seen if the presented results will carry over to a broader population with more participants and other gait patterns. Future studies can even include individuals with gait impairment or paraplegia where control safety is imperative for walking assistance. In addition, future work can entail a more wholistic comparison of control strategies through the addition of other objective measures of safety. This paper acts primarily as a proof-of-concept, showing the assumption made in the theory typically holds true throughout locomotion in a human-exoskeleton system and that feedback torque magnitudes can be reduced in hybrid control over impedance control.

6 Conclusion

This paper presented the experimental application of a hybrid impedance-sliding mode switching controller to the Indego Explorer exoskeleton. The model-based control strategy originally proposed in Ref. [40] is theoretically guaranteed to have lower feedback control signal magnitudes than impedance control. The hybrid control strategy behaves identically to an impedance controller under nominal operating conditions when errors are small but switches to sliding mode control under non-nominal conditions. In this paper, the theory is adjusted to find the condition under which feedback torque control signal magnitudes are lower in the hybrid controller. In addition, the controller is modified using a bilateral mixing strategy to allow for combining the ipsilateral and contralateral controllers, which gives a smooth, continuous control signal during double limb support.

The theory is validated through a perturbed level-treadmill walking experiment with an able-bodied subject, resulting in non-nominal conditions for 15.9% of the experiment. It has been shown that the assumed condition under which feedback torques are lower in hybrid control than impedance control holds true for a large portion of the experiment, failing only 14.3% of the time. A statistically significant reduction of 7.9% in average feedback torques is observed between the hybrid controller and impedance controller, suggesting it may be the safer control strategy. Additionally, the root-mean-square differences in the joint angle ensemble averages were only 0.36° for the hip and 0.64° for the knee. The main results presented in this work demonstrate how the hybrid impedance-sliding mode switching controller is theoretically proven and experimentally validated to have lower feedback torque magnitudes than an impedance controller without drastically affecting gait tracking performance.

Taken altogether, this paper demonstrates that the hybrid controller is practical and comparable to a traditional model-based impedance controller. The hybrid controller provides an extra layer of precaution to impedance control and is a promising alternative control strategy for systems with human-robot or environment-robot interactions.

Acknowledgments The authors would like to thank the individuals at the Human Motion and Control Division at Parker Hannifin Corporation for their technical expertise and support with the Indego Explorer exoskeleton.

Availability of Data and Material Not applicable.

Code or Data Availability Not applicable.

Authors' Contributions C.A.L. developed the controller and composed the manuscript. C.A.L. and A.G. conducted the experiments. R.J.F. provided technical expertise on the exoskeleton. J.T.S. supervised and oversaw the work. All authors reviewed the manuscript.

Funding Not applicable.

Declarations

Ethics Approval Not applicable.

Consent to Participate Not applicable.

Consent for Publication Not applicable.

Conflicts of Interest/Competing Interests Not applicable.

References

1. Lajeunesse, V., Vincent, C., Routhier, F., Careau, E., Michaud, F.: Exoskeletons' design and usefulness evidence according to a systematic review of lower limb exoskeletons used for functional mobility by people with spinal cord injury. Disabil. Rehabil. Assist. Technol. **11**, 535–547 (2016)
2. Swinnen, E., Duerinck, S., Baeyens, J., Meeusen, R., Kerckhofs, E.: Effectiveness of robot-assisted gait training in persons with spinal cord injury: a systematic review. J. Rehabil. Med. **42**, 520–526 (2010)
3. Lee, B.B., Cripps, R.A., Fitzharris, M., Wing, P.C.: The global map for traumatic spinal cord injury epidemiology: update 2011, global incidence rate. Spinal Cord. **52**, 110–116 (2014)
4. Bruns, J., Hauser, W.A.: The epidemiology of traumatic brain injury: a review. Epilepsia. **44**, 2–10 (2003)
5. Maas, A.I.R., Menon, D.K., Adelson, P.D., Andelic, N., Bell, M.J., Belli, A., Bragge, P., Brazinova, A., Büki, A., Chesnut, R.M., Citerio, G., Coburn, M., Cooper, D.J., Crowder, A.T., Czeiter, E., Czosnyka, M., Diaz-Arrastia, R., Dreier, J.P., Duhaime, A.C., et al.: Traumatic brain injury: integrated approaches to improve prevention, clinical care, and research. Lancet Neurol. **16**, 987–1048 (2017)

6. Roozenbeek, B., Maas, A.I.R., Menon, D.K.: Changing patterns in the epidemiology of traumatic brain injury. Nat. Rev. Neurol. **9**, 231–236 (2013)
7. Mahon, C.E., Farris, D.J., Sawicki, G.S., Lewek, M.D.: Individual limb mechanical analysis of gait following stroke. J. Biomech. **48**, 984–989 (2015)
8. Pennycott, A., Wyss, D., Vallery, H., Klamroth-Marganska, V., Riener, R.: Towards more effective robotic gait training for stroke rehabilitation: a review. J. NeuroEng. Rehabil. **9**, 65 (2012)
9. Louie, D.R., Eng, J.J.: Powered robotic exoskeletons in post-stroke rehabilitation of gait: a scoping review. Journal of NeuroEngineering and Rehabilitation. **13**, 53 (2016)
10. Anttila, H., Autti-Rämö, I., Suoranta, J., Mäkelä, M., Malmivaara, A.: Effectiveness of physical therapy interventions for children with cerebral palsy: a systematic review. BMC Pediatr. **8**, 14 (2008)
11. Williams, G.R.: Incidence and characteristics of total stroke in the United States. BMC Neurol. **1**, 1 (2001)
12. Campbell, S.K., Palisano, R.J., Orlin, M.N.: Physical Therapy for Children. Elsevier Saunders, St. Louis, MO (2012)
13. Alexander, M.A., Matthews, D.J., Murphy, K.P.: Pediatric Rehabilitation: Principles and Practice, 5th edn. Demos Medical Publishing, New York, NY (2015)
14. Wren, T.A., Rethlefsen, S., Kay, R.M.: Prevalence of specific gait abnormalities in children with cerebral palsy: influence of cerebral palsy subtype, age, and previous surgery. J. Pediatric Orthopaedics. **25**, 79–83 (2005)
15. Christensen, D., Braun, K.V.N., Doernberg, N.S., Maenner, M.J., Arneson, C.L., et al.: Prevalence of cerebral palsy, co-occurring autism spectrum disorders, and motor functioning – autism and developmental disabilities monitoring network, USA, 2008. Develop. Med. Child Neurol. **56**, 59–65 (2014)
16. Odding, E., Roebroeck, M.E., Stam, H.J.: The epidemiology of cerebral palsy: incidence, impairments and risk factors. Disability Rehabil. **28**, 183–191 (2006)
17. Yilmaz, D., Dehghani-Sanij, A.: A Review of Assistive Robotic Exoskeletons and Mobility Disorders in Children to Establish Requirements of Such Devices for Paediatric Population. In: Reinventing Mechatronics: Proceedings of Mechatronics, Glasgow (2018)
18. Miller, L.E., Zimmermann, A.K., Herbert, W.G.: Clinical effectiveness and safety of powered exoskeleton-assisted walking in patients with spinal cord injury: Systematic review with meta-analysis. Medical Devices (Auckland, N.Z.). **9**, 455–466 (2016)
19. Federici, S., Meloni, F., Bracalenti, M., De Filippis, M.L.: The effectiveness of powered, active lower limb exoskeletons in neurorehabilitation: a systematic review. NeuroRehabil. **37**, 321–340 (2015)
20. Trevino, L., Vatcheva, K., Auer, M., Morales, A., Abdurrahman, L., et al.: A Single-Center Comparison Using Exoskeleton Rehabilitation for Cerebrovascular Accidents and Traumatic Brain Injury in a Cohort of Hispanic Patients. Math. Stat. Sci. Faculty Pub. Pres (2020)
21. Carpino, G., Pezzola, A., Urbano, M., Guglielmelli, E.: Assessing effectiveness and costs in robot-mediated lower limbs rehabilitation: a meta-analysis and state of the art. J. Healthcare Eng. **2018**, 1–9 (2018)
22. Nolan, K.J., Karunakaran, K.K., Ehrenberg, N., Kesten, A.G.: Robotic exoskeleton gait training for inpatient rehabilitation in a young adult with traumatic brain injury. In: Annu. Int. Conf. IEEE Eng. Med. Biol. Soc. (EMBC), IEEE, Honolulu, HI, pp. 2809–2812 (2018)
23. Díaz, I., Gil, J.J., Sánchez, E.: Lower-limb robotic rehabilitation: literature review and challenges. J. Robot. **2011**, e759764 (2011)
24. Bogue, R.: Exoskeletons and robotic prosthetics: a review of recent developments. Ind. Robot. **36**, 421–427 (2009)
25. Viteckova, S., Kutilek, P., Jirina, M.: Wearable lower limb robotics: a review. Biocybern. Biomed. Eng. **33**, 96–105 (2013)
26. Bogue, R.: Robotic exoskeletons: a review of recent progress. Ind. Robot. **42**, 5–10 (2015)
27. Chen, G., Chan, C.K., Guo, Z., Yu, H.: A review on lower extremity assistive robotic exoskeleton in rehabilitation therapy. Crit. Rev. Biomed. Eng. **41**, 343–363 (2013)
28. Marchal-Crespo, L., Reinkensmeyer, D.J.: Review of control strategies for robotic movement training after neurologic injury. J. NeuroEng. Rehabil. **6**, 20 (2009)
29. Jiménez-Fabián, R., Verlinden, O.: Review of control algorithms for robotic ankle systems in lower-limb orthoses, prostheses, and exoskeletons. Med. Eng. Phys. **34**, 397–408 (2012)
30. Ibarra, J.C.P., Siqueira, A.A.G.: Impedance Rontrol of Rehabilitation Robots for Lower Limbs, Review, in: SBR-LARS Robot, pp. 235–240. Symp. Robocontrol, IEEE, Sao Carlos, Sao Paulo, Brazil (2014)
31. Hogan, N.: Impedance control: an approach to manipulation: part I—theory. J. Dyn. Sys. Meas. Control. **107**, 1–7 (1985)
32. Hogan, N.: Impedance control: an approach to manipulation: part II—implementation. J. Dyn. Sys. Meas. Control. **107**, 8–16 (1985)
33. Hogan, N.: Impedance control: an approach to manipulation: part III—applications. J. Dyn. Sys. Meas. Control. **107**, 17–24 (1985)
34. Asada, H., Slotine, J.-J.E.: Robot Analysis and Control. John Wiley & Sons (1986)
35. Mohammadi, A., Gregg, R.D.: Variable Impedance Control of Powered Knee Prostheses Using Human-Inspired Algebraic Curves. Journal of Computational and Nonlinear Dynamics. **14**, (2019)
36. Yu, X., He, W., Li, Y., Xue, C., Li, J., Zou, J., Yang, C.: Bayesian estimation of human impedance and motion intention for human–robot collaboration. IEEE Transactions on Cybernetics. **51**, 1822–1834 (2021)
37. Yu, X., He, W., Li, Q., Li, Y., Li, B.: Human-robot co-carrying using visual and force sensing. IEEE Trans. Ind. Electron. **68**, 8657–8666 (2021)
38. Tran, H.T., Cheng, H., Rui, H., Lin, X., Duong, M.K., Chen, Q.M.: Evaluation of a fuzzy-based impedance control strategy on a powered lower exoskeleton. Int J of Soc Robotics. **8**, 103–123 (2016)
39. Spyrakos-Papastavridis, E., Childs, P.R.N., Dai, J.S.: Passivity preservation for variable impedance control of compliant robots. IEEE/ASME Transactions on Mechatronics. **25**, 2342–2353 (2020)
40. Laubscher, C.A., Sawicki, J.T.: A robust impedance controller for improved safety in human-robot interaction. J. Dyn. Sys., Meas. Control. 1–24 (2021)
41. Søraa, R.A., Fosch-Villaronga, E.: Exoskeletons for all: the interplay between exoskeletons, inclusion, gender, and intersectionality. Paladyn J Behav. Robot. **11**, 217–227 (2020)
42. Dalley, S.A., Hartigan, C., Kandilakis, C., Farris, R.J.: Increased walking speed and speed control in exoskeleton enabled gait. In: IEEE Int. Conf. Biomed. Robot. Biomech. (Biorob), pp. 689–694. IEEE, Enschede (2018)
43. Indego Explorer User Manual Supplement 043–008-000 Rev A, Parker Hannifin Corporation (2018)
44. Parker Hannifin Corporation, Indego Personal Data Sheet (2020)
45. du Bois, J.L., Lieven, N.A.J., Adhikari, S.: Error analysis in trifilar inertia measurements. Exp. Mech. **49**, 533–540 (2009)
46. Korr, A.L., Hyer, P.: A Trifilar Pendulum for the Determination of Moments of Inertia. Frankford Arsenal Research and Development Group Pitman-Dunn Laboratories, Philadelphia, PA (1962)
47. Winter, D.A.: Biomechanics and Motor Control of Human Movement, 4th edn. John Wiley & Sons, Hoboken, NJ (2009)
48. Rose, J., Gamble, J.G.: Human Walking, 3rd Edition. Lippincott Williams & Wilkins (2006)
49. Goo A, Laubscher C, Sawicki JT (2022) Hybrid Zero Dynamics Control of an Underactuated Lower-limb Exoskeleton for Gait

Guidance. Journal of Dynamic Systems, Measurement, and Control. https://doi.org/10.1115/1.4053946
50. Tan, A.H., Godfrey, K.R.: The generation of binary and near-binary pseudorandom signals: an overview. IEEE Trans. Instrum. Meas. **51**, 583–588 (2002)
51. Redd, J., Lyon, C.: Spectral content of NRZ test patterns. Maxim Appl. Note. **3455**(49), 10–14 (2004)
52. The OEIS Foundation, A011673 - OEIS, (n.d.)
53. Winter, D.A.: The Biomechanics and Motor Control of Human Gait: Normal, Elderly and Pathological, 2nd edn. University of Waterloo Press (1991)
54. Laubscher, C.A., Farris, R.J., van den Bogert, A.J., Sawicki, J.T.: An anthropometrically parameterized assistive lower-limb exoskeleton. ASME J. Biomech. Eng. **143**, (2021)
55. Goo, A., Laubscher, C.A., Farris, R.J., Sawicki, J.T.: Design and evaluation of a pediatric lower-limb exoskeleton joint actuator. Actuators. **9**, 16 (2020)

Curt A. Laubscher was born in Cleveland, Ohio, USA, in 1991. He received the B.S. degree in mechanical engineering from Cleveland State University, Cleveland, in 2014, and the Ph.D. degree in mechanical engineering from Cleveland State University, Cleveland, in 2020. Starting in 2014, he has been a Graduate Assistant in the Center for Rotating Machinery Dynamics and Control (RoMaDyC) at Cleveland State University while pursuing his doctorate. Since 2020, he continued as a post-doctorate researcher at RoMaDyC. He is a contributor to a patent for an actuator for a powered pediatric lower-limb exoskeleton. His research interests include robotics, control of dynamical systems, and mechatronics.

Anthony Goo was born in Huntington, West Virginia, USA, in 1994, before moving to Bellingham Washington, USA, in 2000. He received the B.S. degree in mechanical engineering from the University of Notre Dame in 2017 before joining the Center for Rotating Machinery Dynamics and Control (RoMaDyC) at Cleveland State University that same year as a Graduate Assistant while pursuing his Ph.D. His research interests include the development and control of legged exoskeletons, actuator design, and gait rehabilitative and assistive control.

Ryan J. Farris received the B.S. degree in mechanical engineering from Western Kentucky University, Bowling Green, KY, USA, in 2007, and the M.S. and Ph.D. degrees in mechanical engineering from Vanderbilt University, Nashville, TN, USA, in 2009 and 2012, respectively. He is a licensed professional engineer in the states of Tennessee and Ohio. Currently he is the Engineering Manager for Parker Hannifin Corporation's Human Motion and Control Business Unit, Cleveland, OH, USA. He also serves as an adjunct faculty member in the Mechanical Engineering Department, Cleveland State University, Cleveland, OH, USA. His research interests include the design and control of electromechanical devices for medical applications and, in particular, human assistive technologies.

Jerzy T. Sawicki received the M.S. degree in mechanical engineering from the Gdansk University of Technology, Gdansk, Poland, in 1980, the M.S. degree in applied mathematics from the University of Gdansk, Gdansk, in 1986, and the Ph.D. degree in mechanical engineering from Case Western Reserve University, Cleveland, OH, USA, in 1992. He has published more than 250 peer-reviewed papers in the fields of rotor dynamics, tribology, dynamics and vibrations, and advanced control. Dr. Sawicki is the Bently and Muszynska Endowed Chair and Professor and Director of the Center for Rotating Machinery Dynamics and Control (RoMaDyC), Washkewicz College of Engineering, Cleveland State University.